PAPER

High-sensitivity detection of dopamine by biomimetic nanofluidic diodes derivatized with poly(3-aminobenzylamine)†

Gregorio Laucirica, [ID] ‡[a] Yamili Toum Terrones, [ID] ‡[a] Vanina M. Cayón, [ID] [a]
M. Lorena Cortez, [ID] [a] María Eugenia Toimil-Molares,[b] Christina Trautmann,[b,c]
Waldemar A. Marmisollé [ID] *[a] and Omar Azzaroni [ID] *[a]

During the last few years, much scientific effort has been devoted to the control of ionic transport properties of solid state nanochannels and the rational integration of chemical systems to induce changes in the ionic transport by interaction with selected target molecules for (bio)sensing purposes. In this work, we present the construction and functional evaluation of a highly sensitive dopamine-responsive iontronic device by functionalization of bullet-shaped track-etched single nanochannels in PET membranes with poly(3-aminobenzylamine) (PABA). The variety of basic groups in this amino-appended polyaniline derivative allows programming of the ion selectivity of the channel by setting the pH conditions. On the other hand, the amino-pendant groups of PABA become suitable binding sites for the selective chemical reaction with dopamine, leading to a change in the nanochannel surface charge. Thus, the exposure of the PABA-modified nanochannel to dopamine solutions selectively produces changes in the iontronic response. By rationally selecting the conditions for both the dopamine binding step and the iontronic reading, we obtained a correlation between the rectification efficiency and dopamine concentration down to the nanomolar range, which was also successfully interpreted in terms of a simple binding model.

Introduction

Biological ion channels exhibit a sophisticated control of ion transport in response to different environmental changes that allows the accomplishment of a broad variety of physiological functions.[1–5] The ability of living systems to respond to stimuli and process information has encouraged scientists to develop integrated nanosystems displaying similar functions and capabilities.[6–8] In particular, abiotic nanopores and nanochannels have enabled the control and manipulation of the flux of ions in robust and chemically stable systems, leading to the formation of nanopore-platforms with applications in fields such as filtration, nanoelectronics and sensing.[9–11] Nevertheless, beyond the great advances, the exploration of new alternatives to create functional nanodevices remains a goal of paramount relevance.

In the last few years, the design and construction of solid-state nanochannels (SSNs) based on polymer materials have been possible by the use of ion-track etching technology.[12,13] This method offers the possibility to tailor the channel geometry and provides an affordable way to obtain ion current rectifying devices (*i.e.* with diode-like behavior).[14] The phenomenon of ionic current rectification (ICR) stems from the rupture of electrical potential symmetry inside the SSN and as a consequence of the interaction between charged surface groups and ions. ICR is closely related to the ionic selectivity of the system which has major implications for filtration, blue energy harvesting and sensing systems.[15–18] Thus, the modulation of surface group charges and therefore, the selectivity is an important challenge and is considered as a primary goal in the development of nanofluidic devices. In order to attain an accurate control over the surface charges of nanochannels, their surface modification by various techniques has received increasing attention from the scientific community.[6,19,20]

[a]*Instituto de Investigaciones Fisicoquímicas Teóricas y Aplicadas (INIFTA), Departamento de Química, Facultad de Ciencias Exactas, Universidad Nacional de La Plata, CONICET, CC 16 Suc. 4, 1900 La Plata, Argentina.
E-mail: wmarmi@inifta.unlp.edu.ar, azzaroni@inifta.unlp.edu.ar;
http://softmatter.quimica.unlp.edu.ar, www.twitter.com/softmatterlab, www.facebook.com/SoftMatterLaboratory*
[b]*GSI Helmholtzzentrum für Schwerionenforschung, 64291 Darmstadt, Germany*
[c]*Technische Universität Darmstadt, Materialwissenschaft, 64287 Darmstadt, Germany*
†Electronic supplementary information (ESI) available. See DOI: 10.1039/d0nr03634j
‡These authors contributed equally to the work.

Regarding functionalization methods of SSNs, several approaches have been reported.[21,22] Among the different strategies, electrostatic self-assembly of polymers has emerged as a simple and versatile method.[23-25] The appropriate selection of polymers has enabled the design of devices responsive to different stimuli such as pH changes, target molecules, temperature changes, *etc.*[26-28] Electroactive polymers (EPs) have also attracted special attention due to their exceptional features such as ease of synthesis, low cost, and chemical stability.[29,30] Recently, the combination of SSNs and EPs has been exploited for the fabrication of voltage-gated nanofluidic devices. Their remarkable features have promoted the use of these EPs to provide SSNs with a wide variety of functionalities.[11,26,31-36] For example, pH and sugar-gated single nanochannels were fabricated by the functionalization of Au-coated polycarbonate membranes with poly(3-aminophenylboronic acid).[37] Taking advantage of the well-known interactions between borate and sugars and using an aminophenylboronic-derived EP as a modification agent, the authors fabricated a novel device with ionic transport modulated by pH and responsive to fructose, which acts as a chemical effector. In this case the sensing detection mechanism is not based on the electrochemical properties of the polymer, but on the nature of the pendant functional group. Within this line, the rational design of platforms with ionic transport controlled by biorelevant chemical effectors becomes crucial for the generation of nanofluidic systems for biosensing and *in vivo* applications.

Polyaniline (PANI) is another well-studied polymer within the EP family.[38-42] Within PANI derivatives, poly(3-aminobenzylamine) (PABA) is endowed with pendant amino groups that confer additional charges. This not only improves the electroactivity of the polymer at neutral pH compared to PANI, but also yields multifunctional materials by exploiting their functionalization with relevant molecules and biorecognition elements enabled by the reactive primary amino groups.[43-48] Furthermore, PABA has a pH-dependent charge state which makes it an attractive candidate for the development of functional systems based on SSNs. Also, as a polycation, PABA enables both the preparation of stable aqueous dispersions by chemical synthesis and the integration of this material with negative counterparts for the construction of more complex electroactive layer by layer (LbL) assemblies,[49] which supports the idea of using aqueous PABA dispersions for the electrostatic self-assembly on negatively charged surfaces.

On the other hand, benzylamines are known to specifically react with catecholamines in basic aqueous solutions resulting in covalent crosslinking. This is the foundation for the development of catecholamine-sensing platforms based on polybenzylamines.[50-53] In particular, dopamine is a catecholamine that plays a key role in neurotransmission and has important functions in the human body (*e.g.* human metabolism and cardiovascular, central nervous, renal and hormonal systems).[54] Dopamine is critical for signal transmissions to the brain, and an inadequate level of this neurotransmitter has been linked to many neurological disorders, such as Parkinson's disease, drug addiction and attention deficit hyperactivity disorder (ADHD).[55-57] Hence, the development of abiotic dopamine-responsive nanochannel-based devices is of interest from both a basic and an applied perspective.

In this work, we report a new and versatile approach to confer multifunctional properties to SSNs by immobilizing PABA on the surface of a bullet-shaped single nanochannel in a PET membrane *via* electrostatic self-assembly. We demonstrate that PABA-functionalized SSNs act as pH-responsive ionic diodes with good current rectification properties and cyclability. Moreover, we developed a sensing device from the changes in the iontronic response of PABA-functionalized SSN caused by the presence of dopamine. In contrast to the majority of dopamine sensors, the present mechanism is not based on the dopamine electrochemical reaction but on a specific reaction between dopamine and the pendant amine groups of PABA. By rationally selecting the reaction and readout conditions, we were able to fabricate a novel SSN device whose ionic current is sensitive to dopamine concentrations down to the nanomolar range.

Results and discussion

PABA was obtained by a simple chemical batch synthesis in aqueous solution from 3-aminobenzylamine (ABA) and ammonium persulfate as the oxidizing agent, following the protocol reported by Marmisollé *et al.* (Fig. 1a).[49] In contrast to electrodeposition,[58] the synthesis technique applied in this work does not require pre-metallization of the SSN, and is easily extendable to large-scale production. The effectiveness of the synthesis was confirmed by ^{1}H-NMR and ATR-FTIR spectroscopy (Fig. S1 and S2,† respectively).

Bullet-shaped single nanochannels in PET foils were fabricated by the ion-track-etching technique (Fig. S3†).[13] Etching at basic pH values leads to the hydrolysis of the polymer yielding carboxylic groups at the channel surface, which are negatively charged at pH > 4.[59] These negatively charged groups provide a fertile surface where PABA, a polycation that strongly interacts with negatively charged species, can be immobilized.[23] This approach was applied to modify PET membranes by immersion in a PABA aqueous solution at pH = 6. Changes in the wettability of the membranes caused by the electrostatic assembly of PABA were studied by contact angle measurements (Fig. 1b). The contact angle values determined with a 0.1 M KCl solution at pH 3 were ~59° and ~43° before and after the functionalization with PABA, respectively, revealing a clear increase in the hydrophilicity associated with PABA functionalization.

Depending on the sign and magnitude of the surface charges, asymmetric nanochannels rectify ionic currents passing through them.[60] Also, the rectification behavior is highly dependent on factors such as the surface charge, the nanometric size of the nanochannel, the ionic strength, and the presence of specific ionic moieties, among others.[19,28,61,62]
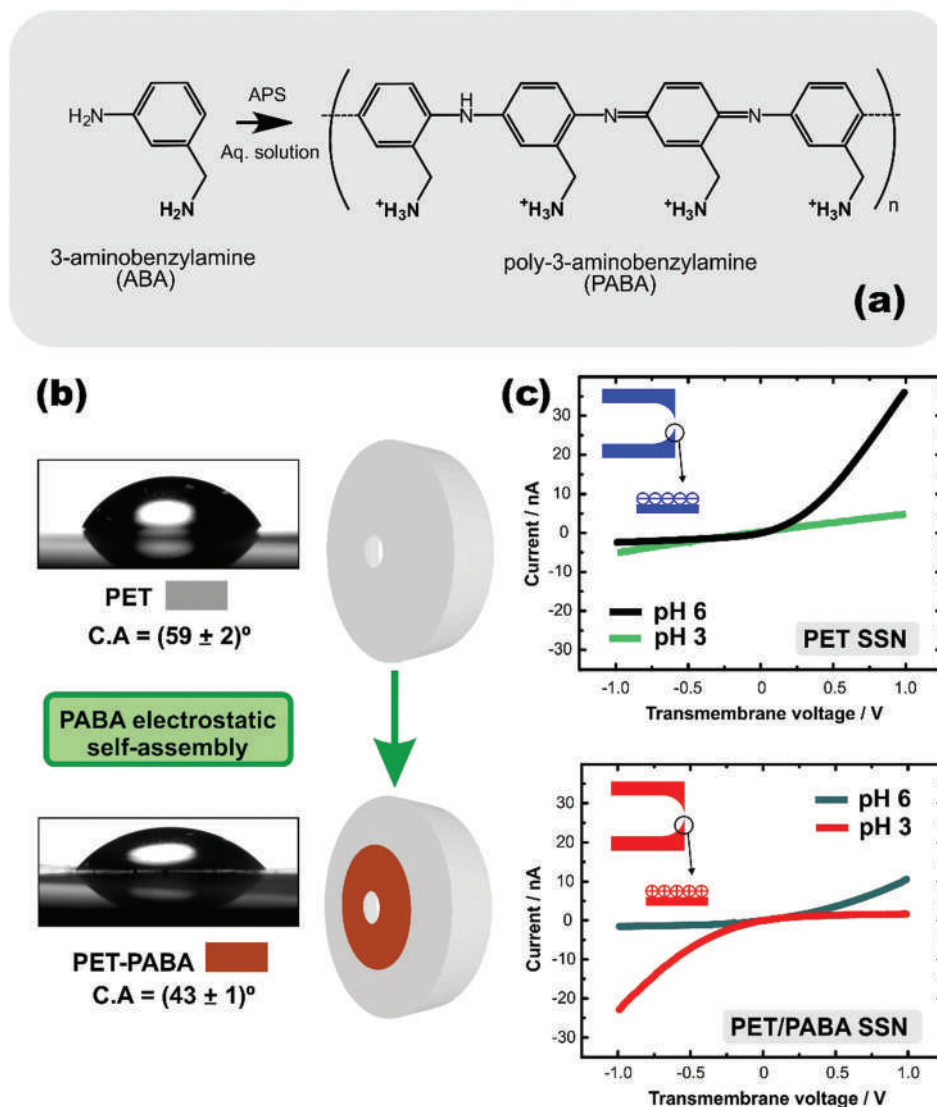
Fig. 1 (a) Reaction scheme: PABA synthesis from the ABA monomer in the presence of ammonium persulfate (APS). (b) Contact angle images before and after the electrostatic self-assembly of PABA (KCl 0.1 M, pH 6). (c) I–V responses of the bare PET SSN (upper figure, KCl 0.1 M, pH 6 and 3) and the PET/PABA SSN (lower figure, KCl 0.1 M, pH 6 and pH 3).

Although the mechanism underlying the rectification of ionic currents is a complex phenomenon, it is possible that charged nanochannels of reduced size are in principle highly selective for ionic species of opposite sign.[63] As shown by Pérez-Mitta *et al.*, the transport number of cations in a bullet-shaped PET SSN (negatively charged after the etching procedure) is close to 0.95 at negative voltages (low conductance states) but close to 0.5 at positive voltages (high conductance states).[16] This means that the occurrence of rectification is associated with a loss of selectivity of the PET SSN at positive potentials, which means that both anions and cations can contribute to the transport of currents.[16] In order to study the iontronic behavior of the nanochannel, current–voltage (I–V) curves were recorded before and after the electrostatic self-assembly of PABA using a four-electrode arrangement. Fig. 1c shows the I–V curves for the PET SSN without any further modification (upper figure) and

after PABA adsorption (PET/PABA SSN) (lower panel). At pH 6, PET SSN exhibits a negatively charged surface provided by the carboxylate groups of PET, and the rectification takes place in a cation-selective mode. In contrast, carboxylates are protonated at pH 3 yielding a neutral nanochannel surface and the device shows ohmic behavior.

After the self-assembly of PABA, PET/PABA SSN exhibits the same rectification mode as PET SSN at pH 6, but a lower current at 1 V and a lower efficiency of rectification. This phenomenon arises as the charges provided by the carboxylate groups of PET are partially compensated by the amino groups of PABA that now decorate the SSN surface. At pH 3, a rectification inversion is clearly seen in the device since amino groups of PABA are mostly charged whereas carboxylates are mostly uncharged, and the ionic transport turns to the anion-selective rectifying regime.

pH responsiveness: selecting charge carriers by pH

In order to study in detail the pH dependence of the PET/PABA SSN, $I–V$ curves at different pH values were measured (experimental set-up is illustrated in the ESI†). Fig. 2a shows the recorded current across the PET/PABA SSN as a function of the transmembrane voltage (V_t). The shape of the $I–V$ curves change with pH following a continuous trend. At pH 2.4, the major part of PABA ionizable groups are protonated, the SSN net charge is positive and, consequently, the ion transport occurs in an anion-selective regime. From the current values at V_t = ±1 V, it is possible to calculate the efficiency of rectification (f_{rec}). The analysis in terms of this parameter is useful since it is closely related to the surface charge.[23] Positive rectification values ($10 < f_{rec} < 1$) are obtained at pH < 3.8 (Fig. 2b). At around pH 4, an isoelectric region can be defined as $f_{rec} \sim$ 1. At pH > 4, an inversion in the rectification direction is observed, *i.e.* the sign of f_{rec} changes. Thus, at pH > 4, the SSNs are negatively charged and they operate in a cation-selective regime. In order to guide the reader, a scheme of the multiple acid–base equilibria inside the PET/PABA SSN is presented in Fig. 2c.

As extensively studied, changes in pH and ionic strength can disassemble multi-layered coatings since these changes in the environmental conditions disrupt or weaken the polyvalent physical interactions (*e.g.*, through electrostatic interactions or by hydrogen bonding) between polyelectrolytes.[64] Therefore, it is crucial to evaluate the robustness of the nanodevice as a pH rectifying nanosensor by testing the reversibility of the iontronic response of a PET/PABA SSN at acidic and basic pH. A reversibility test of the rectification factor f_{rec} presented in Fig. 3 shows that PET/PABA SSN has good reversible pH cyclability between pH 2.5 and 10. The marked difference between the f_{rec} values at acidic and basic pH demonstrates that the device has a good sensitivity to pH changes. In addition, the results reveal highly reproducible and reversible changes in terms of transmembrane ion currents (Fig. 4). Both, the cation and the anion-driven transport are characterized by a significant difference between the high and low conductance states. This suggests that by applying different combinations of pH and transmembrane voltages, a complete regulation of the transmembrane ionic transport can be achieved. Thus, at a fixed voltage there is a pH-induced on–off switching similar to the gating of biological pH-responsive channels.

The robustness of the pH-gated iontronic response can be understood by the nature of the molecular systems integrated
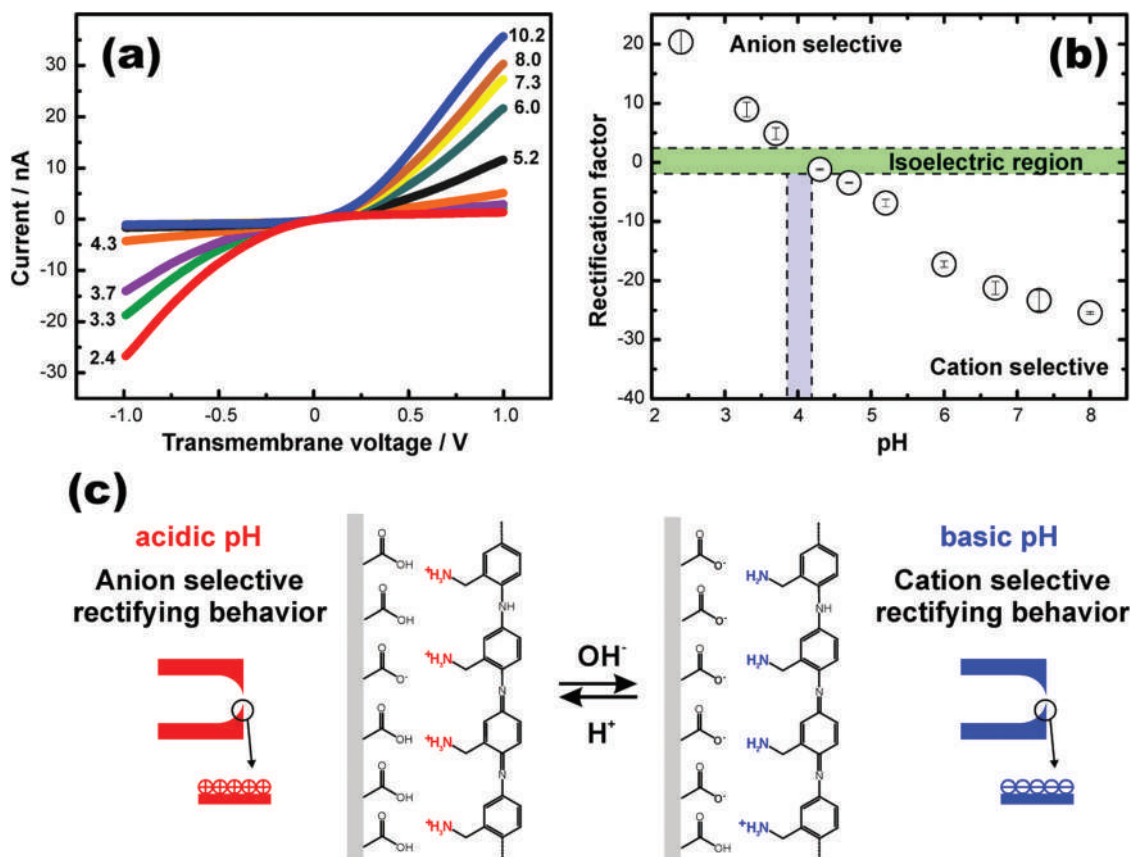

Fig. 2 (a) $I–V$ curves of PET/PABA SSN (KCl 0.1 M) recorded at different pH values from 2.4 to 10.2. (b) Rectification factor *versus* pH: the isoelectric region near pH 4 is shown. (c) Acid–base equilibrium that takes place in PET/PABA SSN walls: schematic representation of the ionizable groups (−COOH from PET and −NH$_2$ from PABA) under acidic and basic pH conditions; the transport changes from anion-selective regime at acidic pH to cation-selective regime at basic pH.
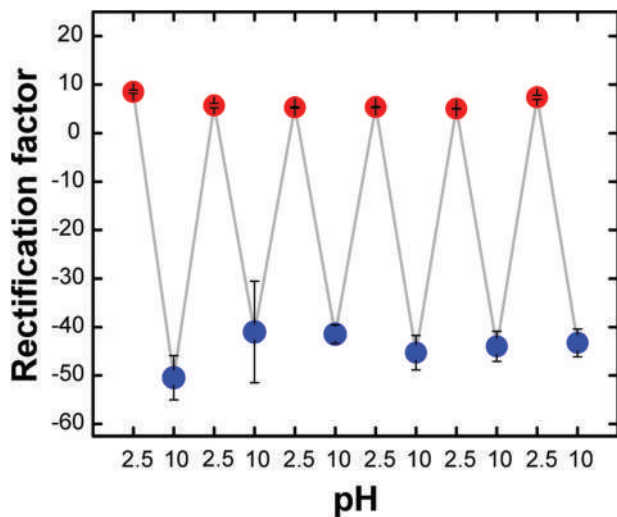
Fig. 3 Reversibility test of rectification factor under cyclic pH changes between 2.5 and 10. All measurements were carried out in 0.1 M KCl, and the pH value was adjusted to 2.5 and 10 with dilute HCl and KOH, respectively. Error bars were calculated by 3 independent measurements.

into the nanochannels. As demonstrated by Monte Carlo simulations for SSNs functionalized by electrostatic self-assembly of polyallylamine (PET/PAH SSN), polyamine is fully charged at low pH, while the carboxylate groups are mostly not.[23] On the other hand, at high pH, carboxylate groups are fully charged while PAH is mostly not. However, even at extreme pH values such as 2 or 10, there are carboxylate and amine groups that remain charged, preventing the polyamine from leaving the

channel. As PABA is an amine-appended polyaniline, the same arguments may hold for the PET/PABA SSN. Moreover, the aromatic polymer backbone allows for another type of interactions that could even improve the stability of the adsorbed PABA chains on the PET membrane in comparison with PAH.

Sub-nanomolar dopamine responsiveness

Previous works have described the selective reaction between catecholamines and benzylamines as an interesting approach for the development of new sensing platforms.[50–53] Fig. 5a shows a general scheme of the reaction where the amine group of benzylamine is covalently bonded to the carbonyl group of a chemically oxidized dopamine. To ensure the formation of oxidized catecholamines, several strategies have been proposed, such as the use of oxidizing agents or adjusting the reaction mixture at pH = 9 to trigger the catechol self-oxidization.[26,50,65] Taking this background into account, we developed a two-step strategy for producing a dopamine-responsive iontronic device: the first step for the dopamine-dependent chemical functionalization and the second step for measuring the iontronic read-out (Fig. 5a and b). Thus, the PET/PABA SSN membrane was first soaked in diluted solutions of dopamine at pH = 9 for 30 minutes. Then, the iontronic readout was performed by acquiring I–V curves in a dopamine-free solution of 0.1 M KCl at pH = 3. The reaction between dopamine and the benzylamine groups of PABA at pH 9 is evidenced by the changes in the iontronic response at pH 3 (Fig. 5c). As previously mentioned, at pH 3 most of the amino groups are positively charged and, consequently, the I–V curve of the untreated PET/PABA membrane displays a high conductance branch at V_t = −1 V (anion-driven rectification). However, soaking in dopa-
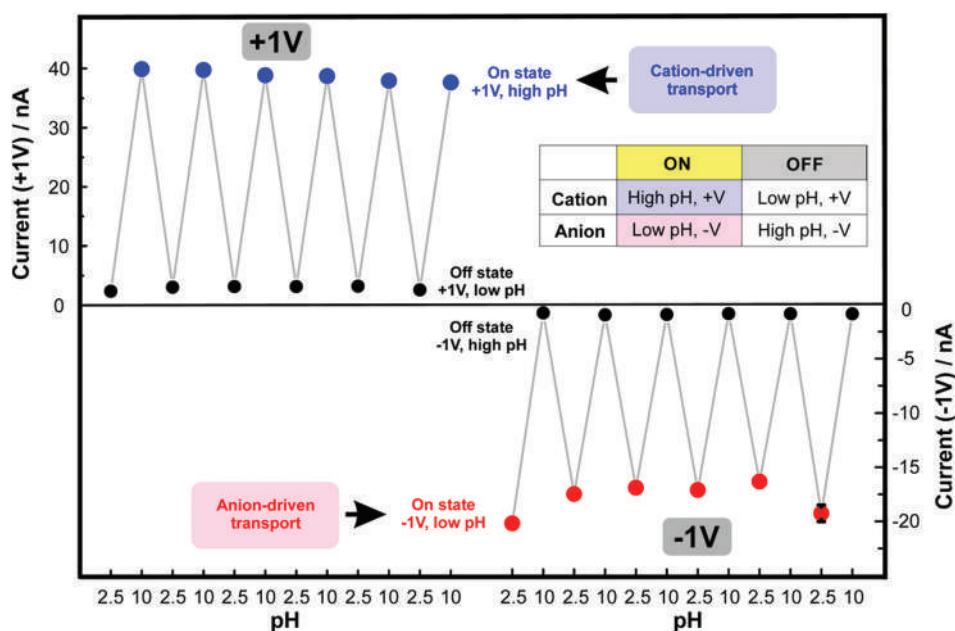

Fig. 4 Reversibility test of the transmembrane ion current (at V_t = +1 V and −1 V) under cyclic pH changes. All measurements were carried out in 0.1 M KCl, and the pH was adjusted to 2.5 and 10 with dilute HCl and KOH, respectively. Selecting specific combinations of pH and voltage allows the control of the transmembrane anion and cation current.
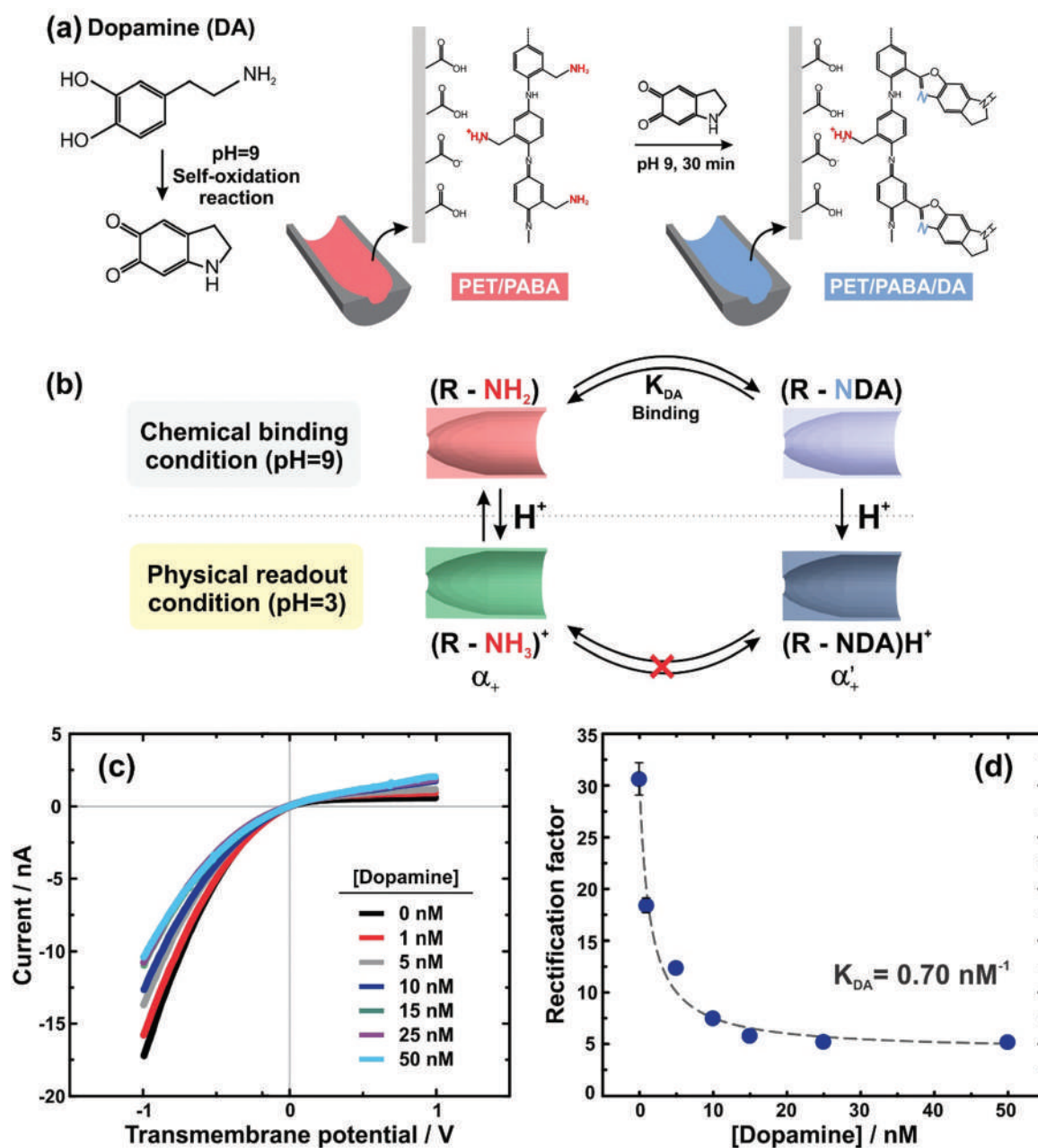
Fig. 5 (a) Scheme of the reaction between DA and PET/PABA SSN. (b) Scheme depicting the chemical species and steps under each pH condition for interpreting the DA-responsiveness in terms of a simple binding model (c) $I-V$ curves of PET/PABA SSN after the exposure to different DA concentrations. (d) Changes in f_{rec} for different DA concentrations. Dashed line corresponds to the fit with the binding model to the experimental data.

mine solutions, even in the nanomolar range, results in both a decline of the current at $V_t = -1$ V (high conductance branch) as well as an increase in the current at $V_t = 1$ V (low conductance branch).

These dopamine-induced changes in the iontronic response are analyzed in terms of f_{rec} as a function of the DA concentration (Fig. 5d). Initially, f_{rec} exhibits a maximum value due to the presence of charged amino groups, but it decreases upon exposure to dopamine. This behavior is caused by the reaction between dopamine and the primary amine groups of PABA which leads to the formation of new imine-groups with a lower

protonation tendency (Fig. 5a)[26] that, in turn, decreases the surface charge density and produces a concomitant loss of f_{rec}. Such a decrease of PABA electrostatic charge due to the reaction with catecholamines has been previously evidenced by XPS and UV/Vis measurements.[52] Finally, f_{rec} reaches a constant value (~5) for dopamine concentrations [DA] > 15 nM that could indicate a saturation range. This limit of the f_{rec} value was maintained even at [DA] = 1 μM (not shown). As presented in Fig. S5,† no appreciable changes in the iontronic response are detected after incubation of a PABA-free membrane (PET) in 1 μM DA at pH 9. This fact allows discarding

both the occurrence of the self-polymerization of DA to polydopamine on the surface (as it is well-reported for much higher DA concentrations[66,67]) and any chemical modification due to the interaction of DA or oxidized DA with the PET membrane. All these results indicate that there exists a specific interaction between DA and PABA.

As recently shown, the iontronic behavior for the interaction between surface amine groups of PET/PAH SSN and different anions can also be explained by a binding formalism.[28,68] In this case, the binding anions were present when recording *I–V* curves and chemical equilibrium considerations were assumed. Here, however, the strategy for sensing dopamine by the iontronic response is more complex as the whole sensing process consists of the first chemical binding step occurring at pH 9 in the presence of DA, and the second physical readout step at which the dopamine-functionalization is determined from changes in the iontronic response at pH 3 (Fig. 5b). The extent to which dopamine binds to amine groups in PABA at pH 9 is characterized by a binding constant, K_{DA}. Dopamine-bound amine sites have a different pK_a value, which results in a lower protonation degree at pH 3, and thus lower f_{rec} values. The rectification factor as a function of the DA concentration is given by (see the ESI† for a detailed derivation):

$$\frac{f_{rec}}{f_{rec}^0} = \frac{1 + \beta K_{DA}[DA]}{1 + K_{DA}[DA]} \qquad (1)$$

where f_{rec}^0 is the initial value before exposure to DA and β is a constant that accounts for the ratio of the protonation degree between DA-bound and free amine sites.

The f_{rec} values shown in Fig. 5d were satisfactorily fitted to eqn (1) and support the proposed binding model. By nonlinear fitting, the DA binding constant was determined to be

0.70 ± 0.2 nM^{-1} ($\beta = 0.14 \pm 0.07$). This value of the affinity constant reveals the sensitivity of the present strategy for sensing DA in the sub-nanomolar range which is comparable with those obtained by other techniques.[69–71]

In order to discard some other possible interaction mechanisms for the changes in the iontronic signal, the selectivity of the response towards DA was evaluated in comparison with other two relevant metabolites: urea and ascorbic acid (AA). Urea belongs to the family of the strong H-bond forming species even at pH 3, which makes it a good candidate to interact with PABA causing the polymer detachment or decreasing its protonation degree. On the other hand, AA has a redox potential close to that of DA and is usually tested as an interfering species in sensor platforms based on the electrochemical detection of DA. If changes in the iontronic response after DA incubation were caused by any redox interaction between DA and the electroactive PABA, similar changes would be expected for AA. Fig. 6 shows the changes in the conductance and rectification factors of PET/PABA SSN after soaking in 10 μM urea and AA solutions comparatively with the changes caused by subsequent incubation in 10 nM and 1 μM DA solutions. To account for membrane-to-membrane variability, the relative conductance (*G*) at $V_t = -1$ V and relative f_{rec} values are presented. In both cases, the relative values provide the ratio of the response parameter after and before the exposure to the analyte solution. Data in Fig. 6 evidence that both, conductance and f_{rec}, do not significantly change after addition of 10 μM AA or urea, while the subsequent exposure of the PET/PABA SSN membrane to 10 nM DA produced a decrease of 50% and 60% in the conductance and rectification factor, respectively. Moreover, these changes were magnified by increasing DA concentration to 1 μM. These results provide strong evidence of the selectivity of the iontronic response towards DA and allow discarding any redox interaction or
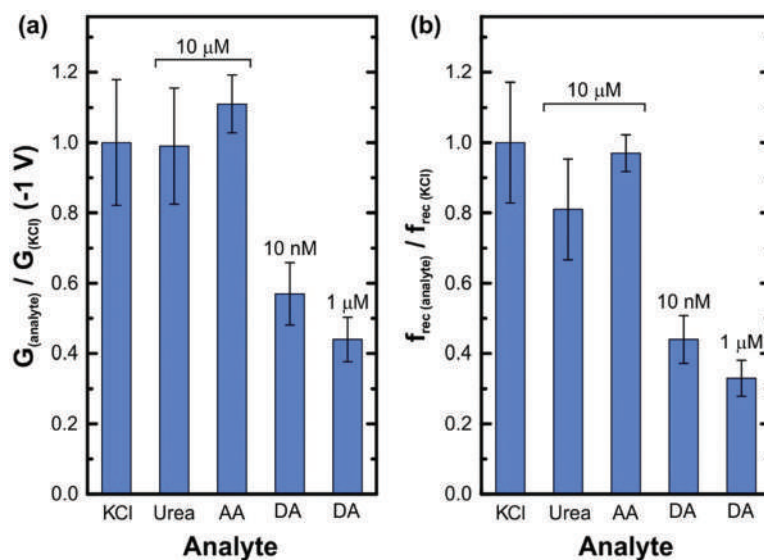

Fig. 6 Selectivity test for PET/PABA SSN membrane without and with exposure to different analytes (a) relative conductance (−1 V) and (b) relative f_{rec}.

analyte-induced polymer detachment. Then, Fig. 6 supports the interaction mechanism proposed in Fig. 5 involving a specific covalent interaction between DA and immobilized benzylamine groups in PET/PABA SSN.

Conclusions

In summary, we have rationally designed and constructed a dopamine-responsive pH-gated nanofluidic diode device by functionalizing a bullet-shaped track-etched PET single nanochannel with an amine-appended polyaniline derivative as a supramolecular building block. In this nanodevice, carboxylate groups on the inner surface of the PET SSN provided a fertile surface where the polycationic PABA could be electrostatically immobilized. Pendant primary amino groups of PABA play a key role not only in the pH responsiveness but also in the DA-effected iontronic behavior of the PET/PABA SSN. The ionic transport properties of the nanochannel are tuned by pH in a remarkably reversible way allowing the selection of the main charge carrier type by pH changes: under acidic conditions, transport occurs in an anion-driven regime whereas at basic pH, the transport is cation-driven. By selecting appropriate chemical functionalization protocols and subsequent readout steps as a sensing strategy, changes in the iontronic response of the PABA-functionalized nanofluidic diode were detected for biologically relevant concentrations (sub-nanomolar range) of dopamine. In addition, the iontronic SSN response was selective to DA compared with other analytes such as ascorbic acid and urea, which may affect the response by redox or hydrogen-bonding interactions with PABA. The role of DA as a chemical effector was then rationalized by the specific chemical interaction between auto-oxidized DA and benzylamine groups from immobilized PABA and explained by a simple binding model. The present simple approach for the functionalization of SSN by ionic self-assembly of PABA opens the door to the exploration and development of further chemical and biochemical sensing platforms by exploiting some advantageous properties of this building block, such as the non-denaturing environment for the electrostatic attachment of enzymes,[45] the chemical richness of the pendant amine groups for performing covalent[44] and non-convalent[46,72,73] integration of other components for further functionalization and its reversible electroactivity and electrocatalytic properties in neutral solutions.[49,58]

Experimental section

Chemicals

KCl, HCl, KOH, NaOH and L-ascorbic acid (AA) were purchased from Anedra. Ammonium persulfate (APS), dopamine (DA) and 3-aminobenzylamine (ABA) were obtained from Sigma-Aldrich. Urea was purchased from Biopack. All chemicals were used as received. All solutions were prepared in MilliQ-water (18.2 MΩ cm).

Nanochannel synthesis

Bullet-shaped nanochannels were prepared by the ion-track-etching method.[13] PET foils (12 μm, Hostaphan RN 12, Hoechst) were irradiated with a single swift heavy ion (~2.2 GeV Au) at the linear accelerator UNILAC at GSI Helmholtzzentrum für Schwerionenforschung (Darmstadt, Germany). The irradiated foils were exposed to an asymmetric surfactant-assisted etching for 6 minutes at 60 °C.[14] One side of the membrane was etched in pure 6 M NaOH (base side), whereas the other side was exposed to 6 M NaOH with the addition of 0.05% Dowfax 2a1 (tip side). Finally, the membranes were kept in MilliQ-water overnight. Under these conditions, the channels with a base diameter of ~900 nm and a tip diameter of ~20 nm were formed (Fig. S3†).

PABA synthesis

PABA was synthesized by chemical oxidation of ABA with APS.[49] With this aim, an aqueous solution of 50 mM ABA and 50 mM APS was prepared and magnetically stirred for 1 hour. In order to purify PABA, 10% KOH was added to the reaction mixture. Then, the solution was centrifuged (7000 rpm, 10 minutes) and the precipitate was re-dispersed in 0.1 M HCl solution. Further details about PABA synthesis and characterization are available in ref. 49.

Channel modification

Modification of PET channel with PABA was carried out by electrostatic self-assembly. With this aim, the membrane was immersed in the PABA solution (5 mg ml^{-1}) at pH = 6 for 4 hours.

Instrumentation

I–V curves were recorded using a potentiostat Gamry Reference 600 with a four-electrode cell. The arrangement consisted of a working electrode (Pt wire), two reference electrodes (Ag/AgCl/ 3 M KCl) and a counter-electrode (Pt wire) and allowed us to relate the changes in the iontronic output to changes on the channel surface. The transmembrane voltage was swept between 1 V and −1 V with a step of 10 mV and a scan rate of 100 mV s^{-1}. In all cases, 0.1 M KCl was used as the supporting electrolyte and the pH value was adjusted by adding HCl and NaOH dilute solutions.

Contact angle measurements were carried out using a Ramé-Hart goniometer (Model 290) by dispensing 2 μl droplets of 0.1 M KCl pH = 3.5 on PET and PET/PABA surfaces. The reported values correspond to the average of three independent measurements.

Rectification factor (f_{rec})

In order to quantify the rectification efficiency, we calculated f_{rec} as follows:

$$f_{rec} = \pm \frac{I(-1\,V\,or\,1\,V)}{I(1\,V\,or\,-1\,V)}. \tag{2}$$

This parameter is useful to correlate the response exhibited in the I–V curves with changes in the surface charge density.[23]

Conflicts of interest

There are no conflicts to declare.

Acknowledgements

References

1 B. Hille, *Ion Channels of Excitable Membranes*, Sinauer Associates, Sunderland, Massachusetts U.S.A, 3rd edn, 2001.

2 H. Zhang, X. Hou, J. Hou, L. Zeng, Y. Tian, L. Li and L. Jiang, *Adv. Funct. Mater.*, 2015, **25**, 1102–1110.

3 L. G. Cuello, J. G. Romero, D. M. Cortes and E. Perozo, *Biochemistry*, 1998, **37**, 3229–3236.

4 L. Heginbotham, M. LeMasurier, L. Kolmakova-Partensky and C. Miller, *J. Gen. Physiol.*, 1999, **114**, 551–559.

5 M. Hirano, Y. Onishi, T. Yanagida and T. Ide, *Biophys. J.*, 2011, **101**, 2157–2162.

6 G. Pérez-Mitta, M. E. Toimil-Molares, C. Trautmann, W. A. Marmisollé and O. Azzaroni, *Adv. Mater.*, 2019, **31**, 1901483.

7 Z. Zhang, L. Wen and L. Jiang, *Chem. Soc. Rev.*, 2018, **47**, 322–356.

8 M. Tagliazucchi and I. Szleifer, *Mater. Today*, 2015, **18**, 131–142.

9 G. Pérez-Mitta, A. S. Peinetti, M. L. Cortez, M. E. Toimil-Molares, C. Trautmann and O. Azzaroni, *Nano Lett.*, 2018, **18**, 3303–3310.

10 P. Wang, M. Wang, F. Liu, S. Ding, X. Wang, G. Du, J. Liu, P. Apel, P. Kluth, C. Trautmann and Y. Wang, *Nat. Commun.*, 2018, **9**, 569.

11 G. Pérez-Mitta, W. A. Marmisollé, C. Trautmann, M. E. Toimil-Molares and O. Azzaroni, *Adv. Mater.*, 2017, **29**, 1700972.

12 P. Apel, *Radiat. Meas.*, 2001, **34**, 559–566.

13 R. Spohr, *Ion Tracks and Microtechnology: Principles and Applications*, Vieweg+Teubner Verlag, 1st edn, 1990.

14 P. Y. Apel, I. V. Blonskaya, S. N. Dmitriev, O. L. Orelovitch, A. Presz and B. A. Sartowska, *Nanotechnology*, 2007, **18**, 305302.

15 Z. S. Siwy, *Adv. Funct. Mater.*, 2006, **16**, 735–746.

16 G. Pérez-Mitta, A. G. Albesa, M. E. Toimil Molares, C. Trautmann and O. Azzaroni, *ChemPhysChem*, 2016, **17**, 2718–2725.

17 J. Cervera, B. Schiedt, R. Neumann, S. Mafé and P. Ramírez, *J. Chem. Phys.*, 2006, **124**, 104706.

18 G. Pérez-Mitta, A. G. Albesa, W. Knoll, C. Trautmann, M. E. Toimil-Molares and O. Azzaroni, *Nanoscale*, 2015, **7**, 15594–15598.

19 G. Pérez-Mitta, A. G. Albesa, C. Trautmann, M. E. Toimil-Molares and O. Azzaroni, *Chem. Sci.*, 2017, **8**, 890–913.

20 G. Pérez-Mitta, L. Burr, J. S. Tuninetti, C. Trautmann, M. E. Toimil-Molares and O. Azzaroni, *Nanoscale*, 2016, **8**, 1470–1478.

21 M. Lepoitevin, T. Ma, M. Bechelany, J. M. Janot and S. Balme, *Adv. Colloid Interface Sci.*, 2017, **250**, 195–213.

22 K. Xiao, L. Wen and L. Jiang, *Small*, 2016, **12**, 2810–2831.

23 G. Pérez-Mitta, A. Albesa, F. M. Gilles, M. E. Toimil-Molares, C. Trautmann and O. Azzaroni, *J. Phys. Chem. C*, 2017, **121**, 9070–9076.

24 C. Lin, C. Combs, Y. Su, L. Yeh and Z. S. Siwy, *J. Am. Chem. Soc.*, 2019, **141**, 3691–3698.

25 M. Ali, B. Yameen, J. Cervera, P. Ramírez, R. Neumann, W. Ensinger, W. Knoll, O. Azzaroni, P. Ramı, R. Neumann, W. Ensinger, W. Knoll and O. Azzaroni, *J. Am. Chem. Soc.*, 2010, **132**, 8338–8348.

26 G. Pérez-Mitta, J. S. Tuninetti, W. Knoll, C. Trautmann, M. E. Toimil-Molares and O. Azzaroni, *J. Am. Chem. Soc.*, 2015, **137**, 6011–6017.

27 Y. Zheng, S. Zhao, S. Cao, S. Cai, X. Cai and Y. Li, *Nanoscale*, 2016, **9**, 433–439.

28 G. Laucirica, G. Pérez-Mitta, M. E. Toimil-Molares, C. Trautmann, W. A. Marmisollé and O. Azzaroni, *J. Phys. Chem. C*, 2019, **123**, 28997–29007.

29 A. G. MacDiarmid, *Angew. Chem., Int. Ed.*, 2001, **40**, 2581–2590.

30 M. E. G. Lyons, *Electroactive Polymer Electrochemistry*, Springer US, Boston, MA, 1st edn, 1994.

31 G. Laucirica, W. A. Marmisollé, M. E. Toimil-Molares, C. Trautmann and O. Azzaroni, *ACS Appl. Mater. Interfaces*, 2019, **11**, 30001–30009.

32 Q. Zhang, Z. Zhang, H. Zhou, Z. Xie, L. Wen, Z. Liu, J. Zhai and X. Diao, *Nano Res.*, 2017, **10**, 3715–3725.

33 Q. Zhang, J. Kang, Z. Xie, X. Diao, Z. Liu and J. Zhai, *Adv. Mater.*, 2017, **30**, 1703323.

34 G. Laucirica, V. M. Cayón, Y. Toum Terrones, M. L. Cortez, M. E. Toimil-Molares, C. Trautmann, W. A. Marmisollé and O. Azzaroni, *Nanoscale*, 2020, **12**, 6002–6011.

35 G. Pérez-Mitta, W. A. Marmisollé, C. Trautmann, M. E. Toimil-Molares and O. Azzaroni, *J. Am. Chem. Soc.*, 2015, **137**, 15382–15385.

36 G. Pérez-Mitta, W. A. Marmisollé, A. G. Albesa, M. E. Toimil-Molares, C. Trautmann and O. Azzaroni, *Small*, 2018, **1702131**, 1–8.

37 G. Pérez-Mitta, W. A. Marmisolle, L. Burr, M. E. Toimil-Molares, C. Trautmann and O. Azzaroni, *Small*, 2018, **14**, 1–8.

38 G. Inzelt, *Conducting Polymers: A New Era in Electrochemistry*, Springer-Verlag, Berlin Heidelberg, 2008.

39 J. Heinze, B. A. Frontana-Uribe and S. Ludwigs, *Chem. Rev.*, 2010, **110**, 4724–4771.

40 S. Bhadra, D. Khastgir, N. K. Singha and J. H. Lee, *Prog. Polym. Sci.*, 2009, **34**, 783–810.

41 G. Ciric-Marjanovic, *Synth. Met.*, 2013, **177**, 1–47.

42 J. Stejskal, M. Trchová, P. Bober, P. Humpolíček, V. Kašpárková, I. Sapurina, M. A. Shishov and M. Varga, *Conducting Polymers: Polyaniline*, John Wiley & Sons Inc., 2015.

43 W. A. Marmisollé, J. Irigoyen, D. Gregurec, S. Moya and O. Azzaroni, *Adv. Funct. Mater.*, 2015, **25**, 4144–4152.

44 G. E. Fenoy, J. M. Giussi, C. von Bilderling, E. M. Maza, L. I. Pietrasanta, W. Knoll, W. A. Marmisollé and O. Azzaroni, *J. Colloid Interface Sci.*, 2018, **518**, 92–101.

45 G. E. Fenoy, W. A. Marmisollé, O. Azzaroni and W. Knoll, *Biosens. Bioelectron.*, 2020, **148**, 111796.

46 G. E. Fenoy, J. Scotto, J. Azcárate, M. Rafti, W. A. Marmisollé and O. Azzaroni, *ACS Appl. Energy Mater.*, 2018, **1**, 5428–5436.

47 M. L. Agazzi, S. E. Herrera, M. L. Cortez, W. A. Marmisollé, C. von Bilderling, L. I. Pietrasanta and O. Azzaroni, *Soft Matter*, 2019, **15**, 1640–1650.

48 S. E. Herrera, M. L. Agazzi, M. L. Cortez, W. A. Marmisollé, C. Bilderling and O. Azzaroni, *Macromol. Chem. Phys.*, 2019, **220**, 1900094.

49 W. A. Marmisollé, E. Maza, S. Moya and O. Azzaroni, *Electrochim. Acta*, 2016, **210**, 435–444.

50 M. Yamaguchi and M. Yoshimura, *Analyst*, 1998, **123**, 307–311.

51 H. Nohta, T. Yukizawa, Y. Ohkura, M. Yoshimura, J. Ishida and M. Yamaguchi, *Anal. Chim. Acta*, 1997, **344**, 233–240.

52 A. Baba, T. Mannen, Y. Ohdaira, K. Shinbo, K. Kato, F. Kaneko, N. Fukuda and H. Ushijima, *Langmuir*, 2010, **26**, 18476–18482.

53 S. Chuekachang, R. Janmanee, A. Baba, S. Phanichphant, S. Sriwichai, K. Shinbo, K. Kato, F. Kaneko, N. Fukuda and H. Ushijima, *Surf. Interface Anal.*, 2013, **45**, 1661–1666.

54 D. S. Kim, E. S. Kang, S. Baek, S. S. Choo, Y. H. Chung, D. Lee, J. Min and T. H. Kim, *Sci. Rep.*, 2018, **8**, 1–10.

55 T. M. Dawson and V. L. Dawson, *Science*, 2003, **302**, 819–822.

56 P. E. M. Phillips, G. D. Stuber, M. L. A. V. Heien, R. M. Wightman and R. M. Carelli, *Nature*, 2003, **422**, 614–618.

57 J. Biederman and S. V. Faraone, *Lancet*, 2005, **366**, 237–248.

58 W. A. Marmisollé, D. Gregurec, S. Moya and O. Azzaroni, *ChemElectroChem*, 2015, **2**, 2011–2019.

59 M. Tagliazucchi and I. Szleifer, *Chemically Modified Nanopores and Nanochannels*, Elsevier Inc., 1st edn, 2016.

60 C. Chad Harrell, Z. S. Siwy and C. R. Martin, *Small*, 2006, **2**, 194–198.

61 C. Wei, A. J. Bard and S. W. Feldberg, *Anal. Chem.*, 1997, **69**, 4627–4633.

62 Z. Siwy, E. Heins, C. C. Harrell, P. Kohli and C. R. Martin, *J. Am. Chem. Soc.*, 2004, **126**, 10850–10851.

63 Z. S. Siwy and C. Martin, *Lect. Notes Phys.*, 2007, **711**, 349–365.

64 D. M. Lynn, *Adv. Mater.*, 2007, **19**, 4118–4130.

65 J. Yang, M. A. Cohen Stuart and M. Kamperman, *Chem. Soc. Rev.*, 2014, **43**, 8271–8298.

66 V. Ball, D. Del Frari, V. Toniazzo and D. Ruch, *J. Colloid Interface Sci.*, 2012, **386**, 366–372.

67 M. Alfieri, L. Panzella, S. Oscurato, M. Salvatore, R. Avolio, M. Errico, P. Maddalena, A. Napolitano and M. D'Ischia, *Biomimetics*, 2018, **3**, 26.

68 G. Laucirica, W. A. Marmisollé and O. Azzaroni, *Phys. Chem. Chem. Phys.*, 2017, **19**, 8612–8620.

69 Y. Huang, Y. Zhang, D. Liu, M. Li, Y. Yu, W. Yang and H. Li, *Talanta*, 2019, **201**, 511–518.

70 Y. Huang, Y. Tang, S. Xu, M. Feng, Y. Yu, W. Yang and H. Li, *Anal. Chim. Acta*, 2020, **1096**, 26–33.

71 W. Yang, Y. Yu, Y. Tang, K. Li, Z. Zhao, M. Li, G. Yin, H. Li and S. Sun, *Nanoscale*, 2017, **9**, 1022–1027.

72 A. Lorenzo, W. A. Marmisollé, E. M. Maza, M. Ceolín and O. Azzaroni, *Phys. Chem. Chem. Phys.*, 2018, **20**, 7570–7578.

73 M. Rafti, W. A. Marmisollé and O. Azzaroni, *Adv. Mater. Interfaces*, 2016, **3**, 1600047.